Research Square

Preprints are preliminary reports that have not undergone peer review.
They should not be considered conclusive, used to inform clinical practice,
or referenced by the media as validated information.

Broadband and Long Landstreamer Seismic Surveying of Metallic Mineral Deposits

Magdalena Markovic

magdalena.markovic@geo.uu.se

Uppsala University

Alireza Malehmir

Uppsala University

Johan Högnäs

Nordic Iron Ore AB

Ronne Hamerslag

Nordic Iron Ore AB

Research Article

Keywords: Broadband landstreamer, hardrock seismics, mineral exploration

Posted Date: November 20th, 2026

DOI: https://doi.org/10.21203/rs.3.rs-11610767/v1

License: This work is licensed under a Creative Commons Attribution 4.0 International License.
Read Full License

Additional Declarations: No competing interests reported.

Broadband and Long Landstreamer Seismic Surveying of Metallic Mineral Deposits

[1]Markovic, M., [1]Malehmir, A., [2]Högnäs, J. and [2]Hamerslag, R.

[1]Department of Earth Sciences, Uppsala University, Villav¨agen 16, Uppsala, 752 36, Sweden

[2]Nordic Iron, Jägarnäsvägen 22, Ludvika, 771 42, Sweden

Corresponding author(s). E-mail(s): magdalena.@geo.uu.se;

Contributing authors: alireza.malehmir@geo.uu.se; johan.hognas@nordiciron.se;

ronne.hamerslag@nordiciron.se;

Abstract

Broadband seismic landstreamers provide a fast data acquisition approach for mineral exploration where both shallow structures and deeper targets may be delineated. This study revisits a three-component (3C) MEMS-based landstreamer concept at the Blötberget iron-oxide deposit in central Sweden, where an earlier landstreamer survey provided one of the first applications of this technology for hardrock mineral exploration. The new acquisition of this study used 220-3C MEMS sensors attached to 11 landstreamer segments with 2 m receiver spacing, giving an active receiver spread of about 440 m. A 500-kg Bobcat-mounted drophammer was operated at 10 m intervals, with two impacts at each source position. The landstreamer was moved along the profile using two overlapping segments between layouts, and the approximately 1.3 km-long seismic profile was acquired within a single day. The vertical-component data reveals the known magnetite- and hematite-rich mineralization together with several deeper reflection packages, a shallow reflection, and an oppositely dipping reflection interpreted as a fault. Comparison with the earlier Blötberget landstreamer survey indicates improved vertical resolution and continuity of the deeper reflections, although the denser receiver sampling and higher seismic fold of the new survey contribute to these differences. The results illustrate how a longer active receiver spread, dense spatial sampling, and a relatively lightweight seismic source can be combined for rapid, a firsthand, broadband seismic acquisition in a hardrock mineral exploration setting.

Key words: Broadband landstreamer, hardrock seismics, mineral exploration

1. Introduction

Reflection seismic methods have increasingly been applied to mineral exploration as exploration targets have moved to greater depths and the need for high-resolution structural information has increased [1–4]. Applications range from imaging structures associated with mineralized systems to detecting mineralized bodies themselves where contrasts in physical properties, particularly density and seismic velocity, produce sufficient seismic impedance contrast [1, 5, 6, 7]. Advances in seismic instrumentation, source technology, acquisition geometry, and processing have expanded the use of the method in hardrock environment [4, 8].

An important development for land near-surface seismic data acquisition is the introduction of towable seismic receiver systems. Early examples include the snowstreamer concept [9], followed by landstreamer systems developed for shallow seismic surveys [10, 11]. Landstreamers have been used in engineering, groundwater, environmental, and infrastructure investigations using both P- and S-wave reflection methods [12–14]. Mounting the receivers on towable platforms reduces the need for conventional receiver planting while maintaining dense spatial sampling. This can considerably shorten field deployment and acquisition time, especially where the receiver spread needs to be moved repeatedly along a profile. A further development was the introduction of broadband digital landstreamers equipped with three-component (3C) MEMS (micro-electromechanical system) sensors [15]. The broadband 3C MEMS system has been applied in urban infrastructure planning [15, 16], groundwater investigations [17], quick-clay landslide studies [18], and more recently geological carbon storage site characterization [19]. These applications include both near-surface investigations and imaging of targets at depths exceeding 1 km.

One of the first applications of this broadband 3C MEMS-based landstreamer to mineral exploration was carried out at the Blötberget iron-oxide deposit in central Sweden [20]. The survey used a 240 m-long landstreamer with 100 MEMS sensors together with a 500-kg Bobcat-mounted drophammer source, and few source points using explosive, for tests. The vertical-component data imaged the known mineralized horizons and indicated reflections extending beyond the mineralization constrained at that time. Since that survey, Blötberget has been investigated using several seismic acquisition and processing approaches, including 2D and sparse 3D reflection seismic surveys and broadband studies

[21–24]. These studies imaged the mineralization and host structures from shallow depths to beyond 850 m, extending below the deepest historical borehole then available (in year 2014).

In the present study, the landstreamer concept is revisited using 220-3C MEMS recorders and an active spread of approximately 440 m. The same 500-kg drophammer source was used, while the acquisition geometry was adapted for a move-along deployment. Here, we focus on the vertical-component data from the entire ~1.3 km-long profile spread acquired within a single day. The resulting seismic section images the known mineralization together with deeper reflection packages, shallow reflections, and an oppositely dipping structure interpreted as a fault. The new results are compared with the earlier Blötberget landstreamer survey to examine how the longer receiver spread and updated acquisition geometry affect the reflection seismic imaging and efficiency in the field.

2. Study site and seismic landstreamer data acquisition

The Blötberget iron-oxide-apatite (IOA) deposit is in the Bergslagen mining district of central Sweden. The mineralization occurs as several sheet-like magnetite- and hematite-rich bodies hosted mainly within Paleoproterozoic felsic metavolcanic rocks, surrounded by younger granitic and pegmatitic intrusions [25–27]. The mineralized bodies generally strike NW-SE and dip moderately towards the southwest [20, 21, 26], a geometry that has been constrained by previous 2D and 3D seismic surveys [20, 21].

Figure 1 shows an aerial image of the study area and the corresponding residual magnetic anomaly map, with the three landstreamer layouts used in the present survey. The pronounced magnetic anomaly on the northern part of the profile is associated with the magnetite-rich Blötberget mineralization and provides additional motive for such position and length of the seismic profile.

A 3C MEMS-based landstreamer system with a 500-kg drophammer was employed for this survey (Figure 2). In total, eleven segments were connected, each comprising of 20 recorders, 2 m apart. The source was generated at every 10 m, collocated with every fifth landstreamer recorder. In addition, 14 source points spaced 20 m apart were acquired beyond the end of the receiver profile, extending the source coverage farther towards the shallower projection of the known mineralization towards the northeast. To improve signal-to-noise ratio, the source pattern was set to be two shots per shot location.

Upon finalizing the layout of eleven segments, nine segments were then moved forward with a four-wheel-drive vehicle, leaving two segments to overlap in the next layout. The overlap is necessary to connect the profile and avoid gap in the fold coverage. A summary of the acquisition parameters is presented in Table 1, including a comparison to the initial survey in 2015 [20].

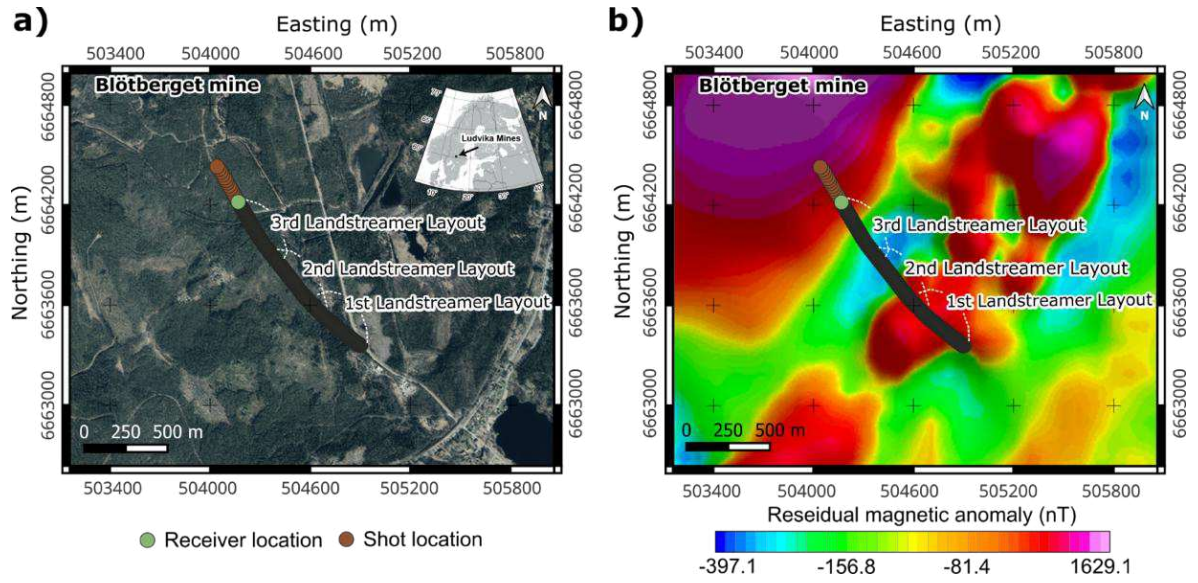


Figure 1. (a) The arial map of the study area with the acquisition layout, and (b) the same profile plotted over the residual magnetic anomaly map. The most prominent magnetic anomaly corresponds to the mineralization zones coming to the surface. Green points show receiver locations, while brown ones are the shot locations.

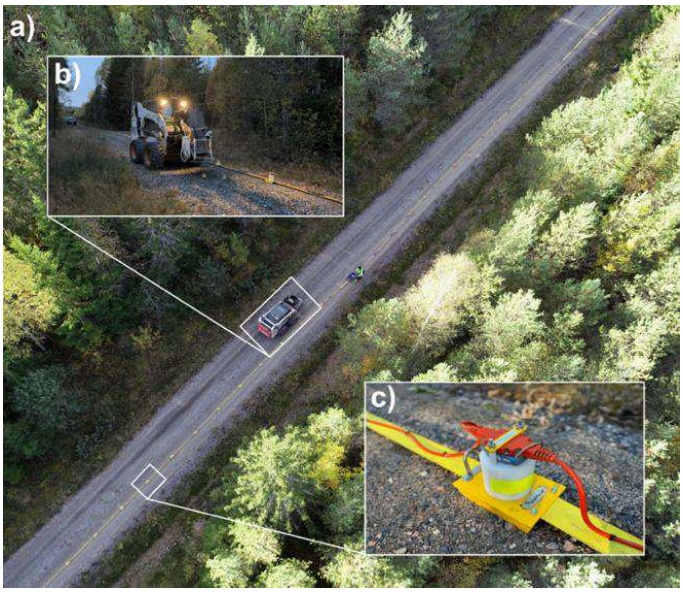


Figure 2. Field photos showing (a) the overall landstreamer layout along the profile, (b) a 500-kg drophammer source, and (c) a 3C MEMS recorder.

Table 1. Summary of acquisition parameters for both initial and present surveys.

Parameter	Inital landstreamer survey	Present study
Receiver system	100 3C MEMS-based cabled landstreamer + 76 nodal receivers (mixed 1C-10Hz gophone and 3C MEMS-based)	220 3C MEMS-based cabled landstreamer
Landstreamer length	240 m	440 m
Receiver spacing	2-4 m	2 m
Number of landstreamer segments	5	11
Move-along overlap	40 m	40 m
Source	500-kg Bobcat-mounted drophammer	500-kg Bobcat-mounted drophammer
Impacts per shot point	3	2
Shot spacing	4 m	10 m
Total profile length	~3.5 km	~1.3 km
Acquisition time	4 days	1 day
Nominal fold	40, including nodal data	22
Outcome	Mineralization imaged to ~850-900 m, possible deeper continuation	Mineralization imaged deeper than 1000 m, deeper underlying reflections, shallow reflection, and fault reflection.

3. Data preparation and processing workflow

Data preparation prior to processing included assigning GPS time stamps of the shot records and DGPS coordinates, removing noisy shots, separating the three components, correcting the zero-time shift, vertically stacking the repeated shots, and defining the acquisition geometry of a bin size 2,6 m x 25 m. Due to the overlapping acquisition layouts, attention was given to maintaining consistent peg numbering. The overlap also produced variable CDP fold coverage.

Refraction static corrections were tested but not retained. First-break picking was challenging, especially at near offsets, and the resulting static corrections introduced large variations between

neighboring stations. After applying them, a prominent shallow reflection became obscured. Place and Malehmir [28] likewise showed that the quality and extent of first-break picks can strongly influence refraction static corrections in hardrock seismic data. Remaining local time shifts were instead corrected using surface-consistent residual reflection statics.

Suppressing the strong surface- and shear-wave energy present in the shot gathers was another important processing step, which helped reveal both shallow and deeper reflection signatures (Figure 3). A band-pass filter of 10-30-100-120 Hz was first applied, followed by spectral equalization using a 50-60-90-110 Hz band-pass and a 30 ms AGC window. Gapped deconvolution was then applied within a 0-800 ms time window, using a filter length of 150 ms and a gap length of 15 ms. To further suppress the coherent shear- and surface-wave energy, a velocity-driven median filter was applied using a horizontal window of 21 traces and a temporal window of 5 ms, with a velocity of 2000 m/s. The filtered wavefield was then subtracted from the original data. An AGC with a 300 ms window was then applied, followed by muting the energy above the first break arrivals.

To obtain the final unmigrated stacked section, an initial NMO velocity of 6000 m/s was applied, followed by two rounds of velocity analysis and surface-consistent residual reflection static corrections. An F-K mute and F-X deconvolution were used to attenuate remaining coherent and random noise, respectively [29]. The NMO-corrected CDP gathers were then combined using diversity stacking, which reduced the contribution of traces dominated by high-amplitude noise. The section was padded with zero traces, migrated using phase-shift migration, and converted from time to depth using the adopted velocity model.

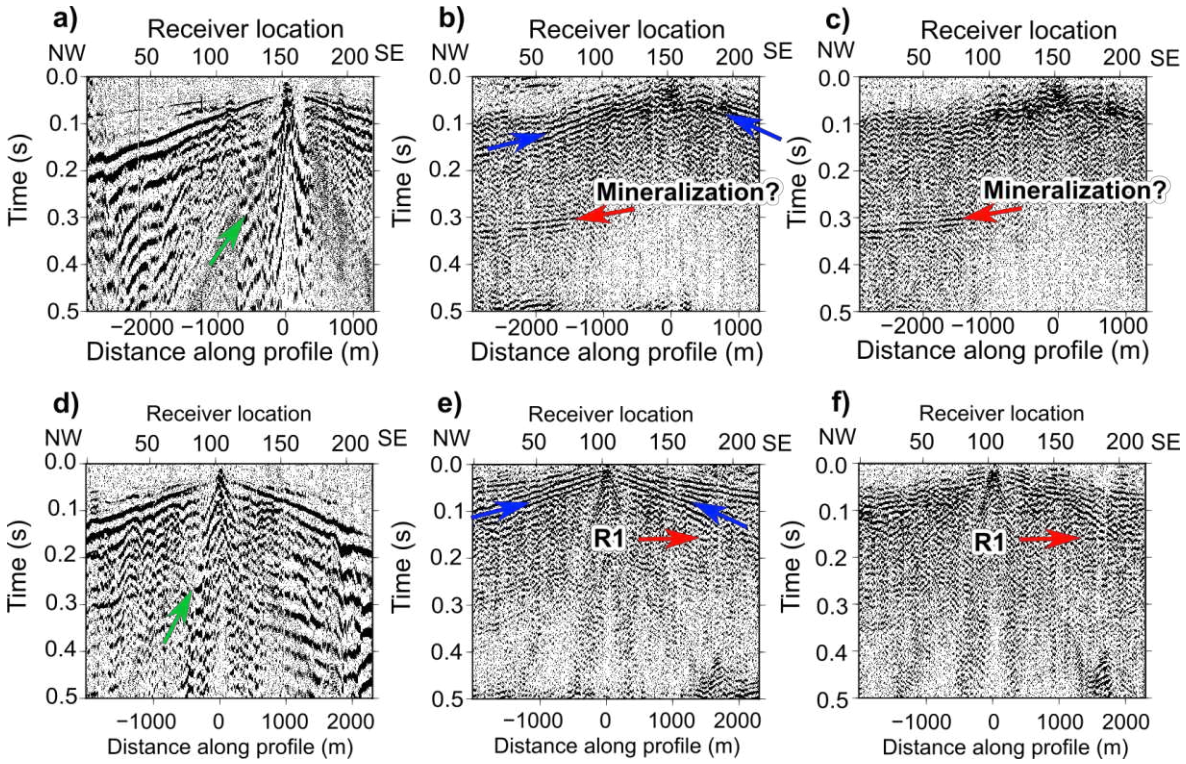


Figure 3. Example shot gathers showing (a-c) the reflection signature of the mineralization and (d-f) a shallow reflection R1. Panels (a, d) show the raw shot gathers, while (b, e) show the data after spectral equalization and deconvolution, which suppressed surface-wave energy (green arrow) and cyclicity in the data. Blue arrows indicate prominent shear-wave arrivals, which were further suppressed via median H-filter in (c, f). The processing also improved the coherency and continuity of both identified reflection signatures.

4. Results and interpretation

The unmigrated stacked section and its corresponding CMP fold distribution is shown in Figure 4. The fold is variable, with decreases at each overlap between repeated landstreamer layouts and towards the NW end of the profile. These lower-fold zones coincide with reduced coherency and continuity in parts of the section. Despite these variations, several distinct reflection features can be identified. The most prominent reflection package corresponds to the known magnetite- and hematite-rich horizons [20–23]. Beneath this package, additional reflections may indicate further mineralized horizons associated with the known mineralization, although their significance and resource potential require further exploration and confirmation [21, 30]. At shallower depths, reflection R1, previously identified in broadband

seismic studies [22, 23], can also be traced. An oppositely dipping reflection intersects the mineralization package and corresponds to a feature previously interpreted as a fault [20–23].

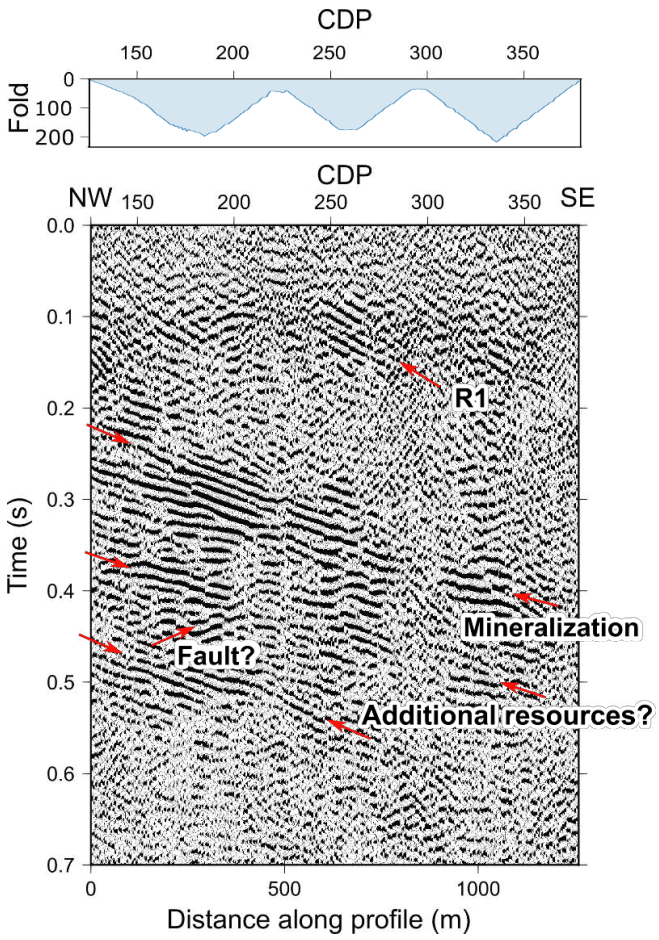


Figure 4. Unmigrated stacked section with the corresponding fold distribution. The unusually high CMP fold is from a trace-sharing approach used during binning to avoid trace loss caused by the crooked acquisition geometry. Red arrows indicate several distinct southeast-dipping reflection signatures, including the main mineralization package, two underlying sets of strong reflections, and the shallow reflection R1. An oppositely dipping reflection intersects the mineralization-related package and corresponds to a feature previously interpreted as a fault.

Following phase-shift migration, the main reflection signatures identified in the unmigrated section remain preserved (Figure 5). Since most reflections dip towards the SE and are imaged close to the edge of the profile, 300 zero traces were padded to the NW side prior to migration to provide sufficient space for their updip repositioning and to reduce edge effects. Some migrated energy, mostly from shallow

events, extends into the padded zone and forms migration smiles; hence, this part of the section is excluded from interpretation.

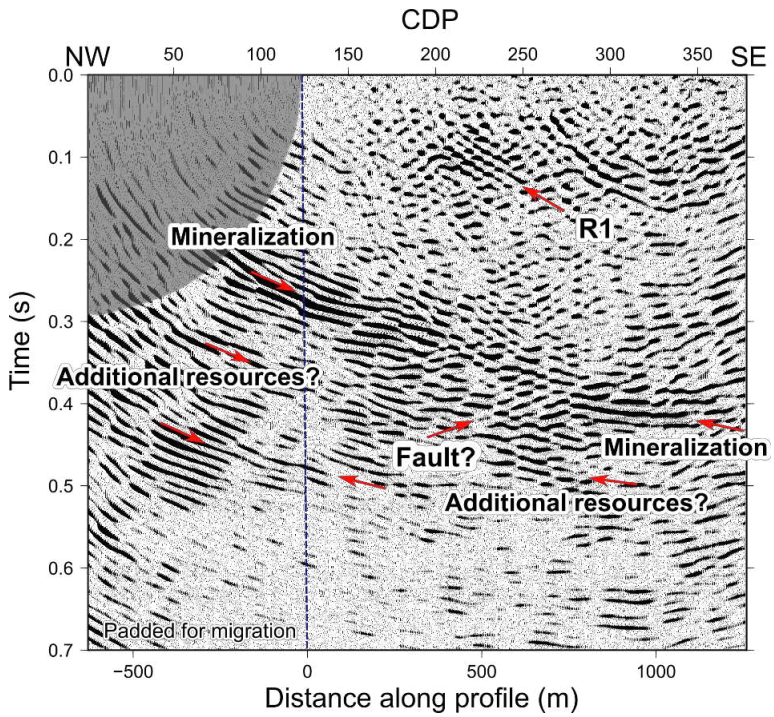
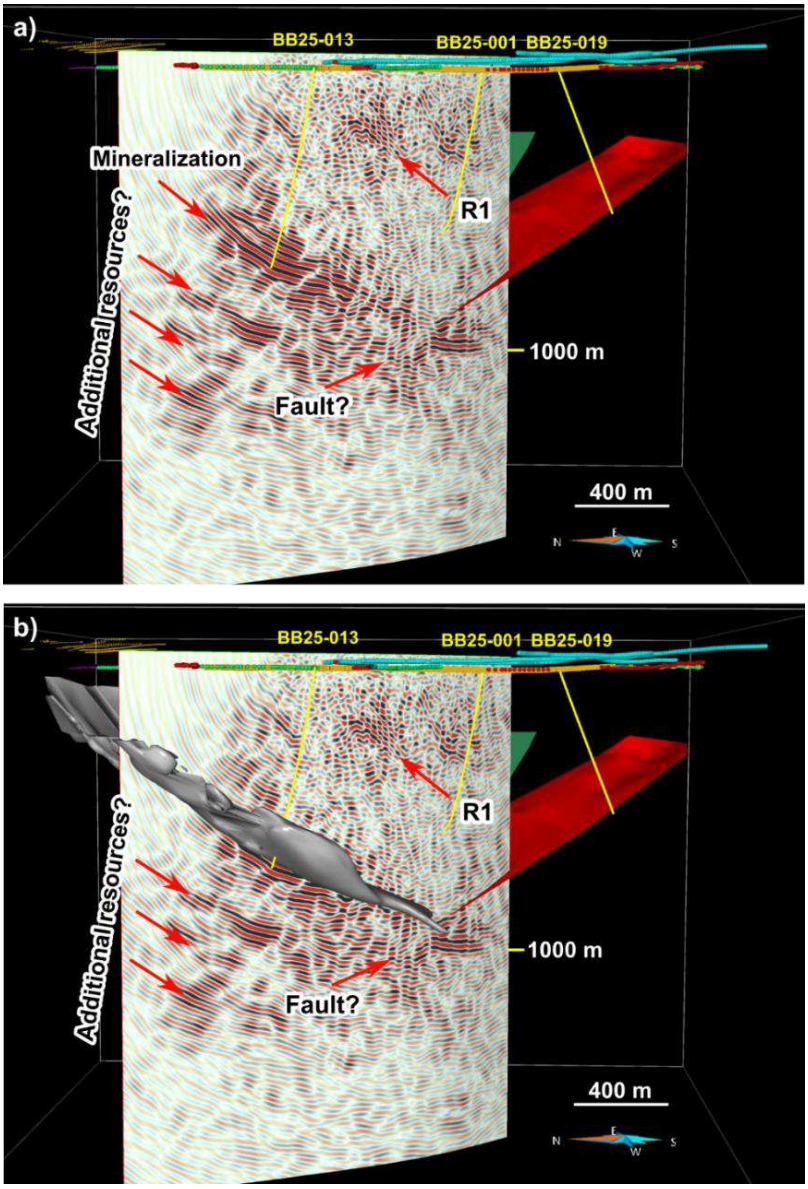


Figure 5. Migrated seismic section showing the main identified features, including the mineralization-related package, underlying sets of reflections, shallow reflection R1, and the opposite dipping reflection-fault. The blue dashed line marks the original NW limit of the seismic profile. The gray-shaded zone to the left represents zero traces padded prior to migration, and it is excluded from interpretation.

Figure 6 shows the migrated and time-to-depth converted section, visualized in 3D with boreholes from the 2025 drilling campaign [31]. The ore block model shown in Figure 6(b) was modelled from borehole information available prior to the 2025 drilling campaign and the sparse 3D seismic [21]. Borehole BB25-001 intersected the mineralization at depths beyond 1000 m, confirming its continuation at depth. The position of the known mineralization reflection agrees well with the modeled mineralization, while the underlying reflection sets remain outside the current geological model and may represent additional mineralized horizons requiring further verification.

The cross-cutting reflection also coincides with the previously interpreted fault plane. Its polarity reversal was examined in detail [24], providing additional seismic support for the fault interpretation.



178

179 **Figure 6.** 3D visualization of (a) the migrated section, where red arrows indicate the main identified
180 reflections, and (b) the migrated section together with the mineralization model (gray). The opposite
181 dipping reflection coincides with the interpreted fault plane (red). Borehole trajectories are shown to
182 illustrate their spatial relationship with the ore model and interpreted seismic features. Note that
183 discovery borehole BB25-001 extends to greater depth behind the 2D seismic section and is only partly
184 visible in this view.

185

186 This interpretation is also supported by the 2025 drilling campaign, where borehole BB25-019
187 intersected several zones of weakness, including a strongly fractured interval at around 700 m depth,
188 suggesting the possible presence of an extensive fault system in this part of the section [32].

At shallower depths, R1 remains geologically uncertain. However, several geophysical observations indicate that this part of the profile is structurally and lithologically complex. Wilczynski et al. [33] found a strong lateral shear-wave velocity contrasts at this location close to the intrusive–metavolcanic contact and to a zone characterized by a pronounced lateral magnetic contrast from high to low residual values (Figure 1b). Shallow reflections were also identified in broadband seismic surveys [23, 24], while a recent multicomponent study revealed a strong S-wavefield diffraction response in the same area [34]. Given all the observations, R1 may be associated with a combination of lithological contrasts, deformation, and local mineralization.

5. Discussion

The 3C MEMS-based landstreamer technology first tested at Blötberget [20] was revisited here with a longer active receiver spread and updated acquisition geometry. While the same 500-kg Bobcat-mounted drophammer was used, the field setup and acquisition geometry were adapted to a longer active receiver spread and more efficient field deployment. The initial survey used a 240 m-long landstreamer with 100 MEMS sensors 2-4 m apart, complemented by nodal receivers and required four days of field acquisition. Even with fewer repeated shots and a wider source spacing, the new dataset images the known mineralization, several underlying reflection packages, the shallow reflection, and the opposite dipping reflection interpreted as a fault. The longer receiver spread, increased channel count, and uniform 2 m receiver spacing provided a more regular acquisition geometry, capturing both shallow and deep geological features within a considerably shorter acquisition time.

Figure 7 compares the unmigrated sections from the earlier and new landstreamer surveys. In both datasets, the main reflection from mineralization is consistent with the modelled mineralization from boreholes. The new section additionally shows several underlying reflection packages that extend beyond the currently modelled mineralization. Their origin remains to be confirmed, but their position makes them relevant targets for further exploration. The comparison also indicates improved vertical resolution in the new section, allowing individual reflection events to be more distinguished.

The move-along acquisition resulted in variable fold along the profile, with decreases at the overlaps between landstreamer layouts. These zones also show lower reflection coherency in the stacked section (Figure 4), indicating that the amount of overlap between layouts needs to be considered when designing similar surveys. Since the two datasets were processed at their original spatial sampling, part of the difference in image resolution may be related to the denser receiver sampling of the new acquisition. A spatial decimation test would be needed to separate this effect from other differences in acquisition and processing.

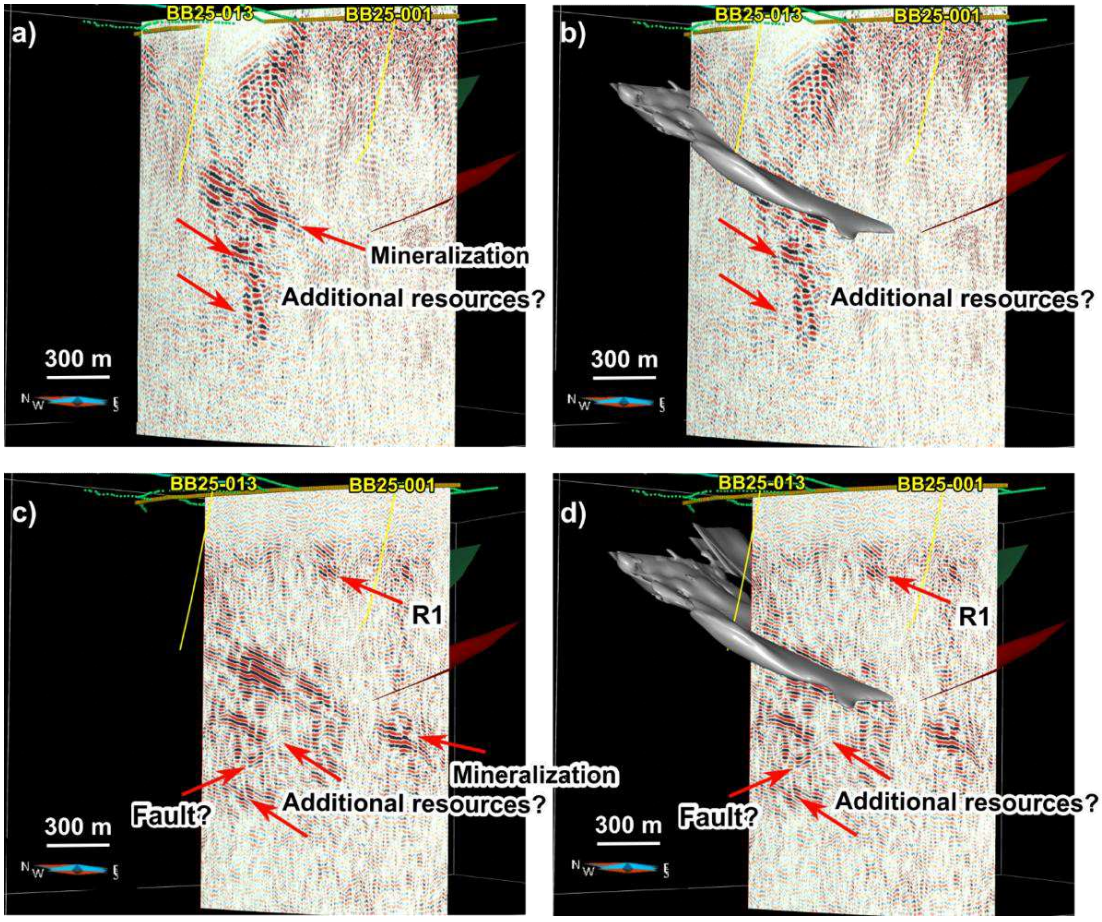


Figure 7. 3D visualization and comparison of unmigrated stacked sections between the (a, b) earlier landstreamer survey [20] and the (c, d) present study. Panels (a, c) show the seismic sections with the main interpreted reflection features, while (b, d) include the ore-body model. Compared with the initial study, where the dominant features are mineralization and underlying reflections, the new section additionally resolves the shallow reflection R1 and the oppositely dipping fault, while the deeper reflection signatures are imaged with greater continuity.

6. Conclusions

The present study shows that a 3C MEMS-based landstreamer combined with a 500-kg drophammer was cost-effective for broadband seismic imaging in a hardrock mineral exploration setting. Using 220 receivers and an active spread of approximately 440 m, about 1.3 km of seismic profile was acquired within a single day. The vertical-component data show the known magnetite- and hematite-rich mineralization, several deeper reflection packages, a shallow reflector, and an oppositely dipping reflection interpreted as a fault. Some of the deeper reflections extend below and beyond the currently modelled mineralization and remain relevant for further exploration.

Revisiting the landstreamer concept more than a decade after its first application at Blötberget also demonstrates how the acquisition approach has developed. Compared with the first landstreamer survey at Blötberget, the new acquisition used a longer active spread, more channels, and a uniform 2 m receiver spacing, while requiring less field time. The new section shows better vertical resolution and more continuous deeper reflections. Part of this difference may, however, be related to the denser receiver sampling and differences in processing between the two datasets. At the transitions between landstreamer layouts, a lower reflection coherency is observed due to variable fold. This indicates that optimal overlap should be considered when planning similar surveys. Nevertheless, the combination of a relatively light seismic source and a mobile landstreamer enabled efficient acquisition while imaging features from the shallow subsurface to depths exceeding 1000 m.

Acknowledgements

This work was partly carried out within the GeoRunner project, funded by Vinnova under reference no. 2024-02691, and within the Smart Exploration Research Center, funded by the Swedish Foundation for Strategic Research under grant agreement no. CMM22-0003. We thank all colleagues, students, and project partners who participated in the fieldwork and contributed to the seismic data acquisition at Blötberget. This is publication number SE26-059.

Supplementary material

Not applicable.

Declarations

Author contribution. MM and AM coordinated the research project and obtained funding. MM and AM designed the survey and took part in the planning and acquisition of the seismic dataset. MM performed seismic data processing and interpretation and wrote the original draft. JH and RH provided access to the study site. All authors contributed to the interpretation and discussion of the results and took part in reviewing and finalizing the manuscript.

Data availability. Data underlying the presented material are available upon request to the corresponding author.

Funding. Magdalena Markovic received funding from VINNOVA; Grant ID 2024-02691.

Alireza Malehmir received funding from Stiftelsen för Strategisk Forskning; Grant ID CMM22-0003.

Competing interests. The authors declare no competing interests.

Third party material. All of the material is owned by the authors and no permission is required.

Consent to participate. Informed consent was obtained from all participants included in the study.

Consent to publish. The authors confirm that participants provided informed consent for publication of the images in Figure 2.

Materials availability. Not applicable.

Code availability. Not applicable.

References

[1] Milkereit B, Eaton DW, Wu J, Perron G, Salisbury MH, Berrer EK, Morrison G. Seismic imaging of massive sulfide deposits: Part II. Reflection seismic profiling. Econ Geol. 1996;91(5):829–34. https://doi.org/10.2113/gsecongeo.91.5.829.

[2] Eaton DW, Milkereit B, Salisbury MH, editors. Hardrock seismic exploration. Tulsa: Society of Exploration Geophysicists; 2003. https://doi.org/10.1190/1.9781560802396.

[3] Adam E, Perron G, Arnold G, Matthews L, Milkereit B. 3D seismic imaging for VMS deposit exploration, Matagami, Quebec. In: Eaton DW, Milkereit B, Salisbury MH, editors. Hardrock seismic exploration. Tulsa: Society of Exploration Geophysicists; 2003. p. 229–46. https://doi.org/10.1190/1.9781560802396.ch15.

[4] Malehmir A, Durrheim R, Bellefleur G, Urosevic M, Juhlin C, White DJ, Milkereit B, Campbell G. Seismic methods in mineral exploration and mine planning: a general overview of past and present case histories and a look into the future. Geophysics. 2012;77(5):WC173–90. https://doi.org/10.1190/geo2012-0028.1

[5] Salisbury MH, Milkereit B, Bleeker W, Adair R, Matthews L. Seismic imaging of massive sulfide deposits: Part I. Rock properties. Econ Geol. 1996;91(5):821–8. https://doi.org/10.2113/gsecongeo.91.5.821

[6] Maries G, Malehmir A, Bäckström E, Schön M, Marsden P. Downhole physical property logging for iron-oxide exploration, rock quality, and mining: an example from central Sweden. Ore Geol Rev. 2017;90:1–13. https://doi.org/10.1016/j.oregeorev.2017.10.012

[7] Van Santvliet F, Markovic M, Malehmir A, et al. Physical property analysis for deep seismic targeting of the Viscaria Cu-Fe deposit, northern Sweden. In: Near Surface Geoscience Conference & Exhibition 2026. European Association of Geoscientists & Engineers; 2026. https://doi.org/10.3997/2214-4609.202620037

[8] Malehmir A, Markovic M, Papadopoulou M, Högdahl K, Ask M, Strømme M, Pitcairn I, Martin T, Zack T, Majka J, Svensson M, Hamerslag R. Smart Exploration Research Centre: knowledge and innovation for exploration of critical raw materials. First Break. 2024;42(8):89–91. https://doi.org/10.3997/1365-2397.fb2024068

[9] Eiken O, Degutsch M, Riste P, Rød K. Snowstreamer: an efficient tool in seismic acquisition. First Break. 1989;7(9):374–8. https://doi.org/10.3997/1365-2397.1989021.

[10] van der Veen M, Green AG. Land streamer for shallow seismic data acquisition: evaluation of gimbal-mounted geophones. Geophysics. 1998;63(4):1408–13. https://doi.org/10.1190/1.1444442.

313 [11] van der Veen M, Spitzer R, Green AG, Wild P. Design and application of a towed land-streamer
314 system for cost-effective 2-D and pseudo-3-D shallow seismic data acquisition. Geophysics.
315 2001;66(2):482–500. https://doi.org/10.1190/1.1444939.
316 [12] Pugin AJM, Larson TH, Sargent SL, McBride JH, Bexfield CE. Near-surface mapping using SH-
317 wave and P-wave seismic land-streamer data acquisition in Illinois, U.S. Lead Edge.
318 2004;23(7):677–82. https://doi.org/10.1190/1.1776740.
319 [13] Pullan SE, Pugin AJM, Hunter JA, Cartwright T, Douma M. Application of P-wave seismic
320 reflection methods using the Landstreamer/Minivib system to near-surface investigations. In:
321 21st EEGS Symposium on the Application of Geophysics to Engineering and Environmental
322 Problems; 2008. https://doi.org/10.3997/2214-4609-pdb.177.89.
323 [14] Pugin AJM, Pullan SE, Hunter JA, Oldenborger GA. Hydrogeological prospecting using P- and
324 S-wave landstreamer seismic reflection methods. Near Surf Geophys. 2009;7(5–6):315–28.
325 https://doi.org/10.3997/1873-0604.2009033.
326 [15] Brodic B, Malehmir A, Juhlin C, Dynesius L, Bastani M, Palm H. Multicomponent broadband
327 digital-based seismic landstreamer for near-surface applications. J Appl Geophys.
328 2015;123:227–41. https://doi.org/10.1016/j.jappgeo.2015.10.009.
329 [16] Malehmir A, Zhang F, Dehghannejad M, Lundberg E, Döse C, Friberg O, Brodic B, Place J,
330 Svensson M, Möller H. Planning of urban underground infrastructure using a broadband seismic
331 landstreamer—tomography results and uncertainty quantifications from a case study in
332 southwestern Sweden. Geophysics. 2015;80(6):B177–92. https://doi.org/10.1190/geo2015-
333 0052.1.
334 [17] Brodic B, Malehmir A, Pugin A, Maries G. Three-component seismic land streamer study of an
335 esker architecture through S- and surface-wave imaging. Geophysics. 2018;83(6):B339–53.
336 https://doi.org/10.1190/geo2017-0747.1.
337 [18] Pertuz T, Malehmir A. Ultrahigh-resolution 9C seismic survey in a landslide prone area in
338 southwest of Sweden. Geophys J Int. 2023;235(3):2094–106.
339 https://doi.org/10.1093/gji/ggad346.

[19] Malehmir A, Markovic M, Abramovitz TJ, Gregersen U. Geological carbon storage site characterization using a dual element seismic recording technology. Sci Rep. 2025;15:12937. https://doi.org/10.1038/s41598-025-96012-8.

[20] Malehmir A, Maries G, Bäckström E, Schön M, Marsden P. Developing cost-effective seismic mineral exploration methods using a landstreamer and a drophammer. Sci Rep. 2017;7:10325. https://doi.org/10.1038/s41598-017-10451-6.

[21] Markovic M, Maries G, Malehmir A, von Ketelhodt J, Bäckström E, Schön M, Marsden P. Deep reflection seismic imaging of iron-oxide deposits in the Ludvika mining area of central Sweden. Geophys Prospect. 2020;68(1):7–23. https://doi.org/10.1111/1365-2478.12855.

[22] Malehmir A, Markovic M, Marsden P, Gil A, Buske S, Sito L, Bäckström E, Sadeghi M, Lüth S. Sparse 3D reflection seismic survey for deep-targeting iron oxide deposits and their host rocks, Ludvika Mines, Sweden. Solid Earth. 2021;12:483–502. https://doi.org/10.5194/se-12-483-2021.

[23] Pertuz T, Malehmir A, Bos J, Brodic B, Ding Y, de Kunder R, Marsden P. Broadband seismic source data acquisition and processing to delineate iron oxide deposits in the Blötberget mine-central Sweden. Geophys Prospect. 2021;70(1):79–94. https://doi.org/10.1111/1365-2478.13159.

[24] Gyger L, Malehmir A, Manzi M, Vivin L, Lépine J, Kaslilar A, Valishin O, Marsden P, Hamerslag R. Broadband seismic data acquisition and processing of iron oxide deposits in Blötberget, Sweden. Geophys Prospect. 2025;73(1):80–95. https://doi.org/10.1111/1365-2478.13648

[25] Allen RL, Lundström I, Ripa M, Christofferson H. Facies analysis of a 1.9 Ga, continental margin, back-arc, felsic caldera province with diverse Zn-Pb-Ag-(Cu-Au) sulfide and Fe oxide deposits, Bergslagen region, Sweden. Econ Geol. 1996;91(6):979–1008. https://doi.org/10.2113/gsecongeo.91.6.979

[26] Stephens MB, Ripa M, Lundström I, Persson L, Bergman T, Ahl M, Wahlgren CH, Persson PO, Wickström L. Synthesis of the bedrock geology in the Bergslagen region, Fennoscandian Shield, south-central Sweden. Uppsala: Geological Survey of Sweden; 2009. SGU Ba 58.

[27] Almqvist BSG, Björk A, Mattsson HB, Hedlund D, Gunnarsson K, Malehmir A, Högdahl K, Bäckström E, Marsden P. Magnetic characterisation of magnetite and hematite from the Blötberget apatite-iron-oxide deposits (Bergslagen), south-central Sweden. Can J Earth Sci. 2019;56(9):948–57. https://doi.org/10.1139/cjes-2018-0183

[28] Place J, Malehmir A. Using supervirtual first arrivals in controlled-source hardrock seismic imaging—well worth the effort. Geophys J Int. 2016;206(1):716–30. https://doi.org/10.1093/gji/ggw176

[29] Yilmaz Ö. Seismic data analysis: processing, inversion, and interpretation of seismic data. 2nd ed. Tulsa: Society of Exploration Geophysicists; 2001. https://doi.org/10.1190/1.9781560801580

[30] Markovic M, Malehmir A, Högnäs J, Hamerslag R. Sparse 3D reflection seismic survey for imaging lateral extensions of iron-oxide mineralization at Blötberget, Sweden. In: Near Surface Geoscience Conference & Exhibition 2026. European Association of Geoscientists & Engineers; 2026. p. 1–5. https://doi.org/10.3997/2214-4609.202620209

[31] Malehmir A, Markovic M, Hamerslag R, Högnäs J. Building confidence at depth: over a decade of innovation in deep mineral targeting. First Break. 2026;44(8):25–32. https://doi.org/10.3997/1365-2397.fb2026057

[32] Wilczynski Z, Kaslilar A, Malehmir A, Juhlin C, Markovic M, Gyger L, Manzi M. Performance of untrenched surface-DAS in near-surface seismic exploration: a comparison with conventional sensors. Geophys J Int. 2026;245(2):ggag082. https://doi.org/10.1093/gji/ggag082

[33] Markovic M, Malehmir A, Manzi MSD, Hamerslag R. Feasibility of multicomponent reflection seismic imaging for direct targeting of metallic mineral deposits. Geophysics. 2025;90(6):B357–66. https://doi.org/10.1190/geo2025-0065.1